

Investigating the H I mass-size relation using the SIMBA cosmological simulations.

Omphile Rabyang,^{1*} Ed Elson,¹

¹*Department of Physics & Astronomy, University of the Western Cape, Robert Sobukwe Rd, Bellville, 7535, South Africa*

Accepted XXX. Received YYY; in original form ZZZ

ABSTRACT

Observational studies have established a remarkably tight power-law relationship between the H I masses and sizes of late-type galaxies, known as the H I mass–size relation. This relation has been shown to persist across various models of a galaxy’s H I surface density profile. Using the SIMBA cosmological simulations, we investigate the robustness of this relation under different feedback prescriptions, including cases where specific feedback mechanisms are absent. While the global properties of galaxies are significantly affected by changes in feedback, the H I mass–size relation remains intact. Moreover, its parameters consistently align with the best available empirical measurements. We analyse the H I mass distributions of galaxies and demonstrate that, regardless of the feedback scenario, galaxies within a given H I mass bin exhibit outer H I radial profiles well-approximated by an exponential function. Furthermore, the exponential decline rate remains remarkably similar across different physical prescriptions. This behaviour is only valid within the $\sim 1 \text{ M}_\odot \text{ pc}^{-2}$ contour. We attribute the persistence of the H I mass–size relation to this inherent self-similarity in the H I mass distributions.

Key words: H I mass–size relation – SIMBA cosmological simulations – Feedback prescriptions

1 INTRODUCTION

The spatial distribution of neutral atomic hydrogen (H I) in galaxies provides crucial insights into their assembly histories, mechanisms of gas accretion and the role of feedback processes in shaping their evolution. Among the most robust observational findings in this context is the tight empirical relation between a galaxy’s H I mass and its spatial extent, known as the H I mass–size relation (H I MSR) (Broeils & Rhee 1997; Wang 2016). This relation is well described by a single power law over several orders of magnitude in H I mass and is characterized by remarkably low scatter, typically around 0.06 dex, indicating a high degree of regularity across diverse galaxy populations.

The universality and tightness of the H I MSR are widely interpreted as evidence for structural self-similarity in H I discs, suggesting that similar physical mechanisms govern the distribution of atomic hydrogen across a broad range of galaxy types and environments (Wang et al. 2014; Stevens et al. 2019). Observational studies have found that the average H I surface density, $\Sigma_{\text{H I}}(r)$, within the H I radius is nearly constant for most galaxies, further supporting the idea of a common underlying process.

Despite this, the extent to which feedback processes—arising from both stellar processes and active galactic nuclei (AGN) activity—might disrupt or regulate the H I MSR remains an open question. Theoretical and semi-analytic models suggest that feedback can influence the structure of H I discs, but the observed tightness of the H I MSR places strong constraints on the degree of disruption

permissible. Recent hydrodynamical simulations, such as EAGLE (Crain et al. 2015; Bahé et al. 2016), have shown that strong AGN feedback can suppress central H I densities and potentially induce deviations from the canonical H I MSR, highlighting the need to isolate the influence of individual feedback channels.

In this study, we investigate the impact of various feedback prescriptions on the H I MSR using the SIMBA (Davé et al. 2019) suite of cosmological hydrodynamical simulations. SIMBA incorporates both stellar and AGN feedback, including radiative, jet, and X-ray heating modes, enabling a systematic exploration of their respective roles. We analyse four variants of the simulation: a fiducial run with full feedback physics, and three others in which one or more AGN feedback modes are selectively disabled. For each scenario, we measure the global H I MSR and examine the radial H I surface density profiles to assess whether the observed universality arises from structural self-similarity and whether this is preserved under different feedback regimes.

This paper is structured as follows. In Section 2, we describe the simulation and the different variants. Section 3 focuses on the methodology. Section 4 presents the sample selection for the H I MSR. The results and discussion are presented in Section 5 and 6, respectively.

2 SIMBA SIMULATIONS

In this study, we use the SIMBA suite of cosmological simulations (Davé et al. 2019), a descendant of the MUFASA simulation (Davé, Thompson & Hopkins 2016), which is built upon the meshless finite

* E-mail: 4115981@myuwc.ac.za

mass (MFM) hydrodynamics solver of the GIZMO code (Hopkins 2015). SIMBA incorporates updated physics for black hole growth and feedback and includes prescriptions for star formation, black hole seeding and accretion, as well as stellar and AGN feedback. It also accounts for radiative cooling, photoionization heating, metal cooling, and the out-of-equilibrium evolution of primordial elements via the grackle-3.1 library (Smith et al. 2017). SIMBA calculates molecular hydrogen content on-the-fly and uses a subgrid model for star formation, which allows it to account for the molecular phase of gas.

The simulation models black hole accretion using both Bondi-Hoyle accretion for hot gas and torque-limited accretion for cold gas (Anglés-Alcázar et al. 2017), improving realism compared to other simulations that use only Bondi accretion. There are two main types of feedback in SIMBA: stellar feedback and AGN feedback. Stellar feedback incorporates supernovae, radiation pressure, and stellar winds, while AGN feedback operates in three modes¹:

(i) **AGN Winds:** Active when the Eddington ratio is high ($f_{\text{Ed}} > 0.2$). In this regime, black holes (BH) drive mass-loaded winds with velocities of $\sim 1000 \text{ km s}^{-1}$, ejected radially in the direction of the angular momentum of the inner accretion disk. These outflows are launched with zero opening angle and do not alter the gas temperature at injection.

(ii) **AGN Jets:** Fully activated at low Eddington ratios ($f_{\text{Ed}} < 0.02$) for BH with masses $> 10^{7.5} M_{\odot}$. This mode produces highly collimated, bipolar jets with zero initial aperture and velocities reaching up to 7000 km s^{-1} . The outflowing gas is heated to the halo virial temperature prior to ejection. In the intermediate regime ($0.02 < f_{\text{Ed}} < 0.2$), wind velocity increases smoothly as f_{Ed} decreases.

(iii) **X-ray Heating:** Activated concurrently with jet mode. Based on the model of Choi et al. (2012), this mode differentiates its treatment of gas by density. For non-interstellar medium (ISM) gas, the injected X-ray energy directly increases the temperature. For ISM gas, half the energy is used to impart a radial velocity kick, while the remainder is deposited as heat. This feedback component is important for suppressing residual star formation in quenched galaxies.

The AGN feedback implementations in SIMBA are designed to reproduce the observed bimodality in black hole growth in AGN, as reported by Heckman & Best (2014). SIMBA also implements a two-mode kinetic AGN feedback, with radiative winds at high accretion rates and jet feedback at lower accretion rates. The combination of these feedback mechanisms helps to quench massive galaxies and match observed galaxy populations and BH growth. Finally, SIMBA models the transformation of ionised gas into atomic and molecular phases by incorporating self-shielding and using a prescription for the H_2 fraction based on the gas metallicity, as described in the Rahmati et al. (2013). Since SIMBA has been extensively described in previous works, we provide a brief overview of the main simulation parameters and refer the reader to Davé et al. (2019) for a more detailed description. Additional information on the feedback mechanism modes of SIMBA can also be found in Ward et al. (2022); Christiansen et al. (2020); Khrykin et al. (2024).

In these simulations, halos are identified on the fly using a 3-D friends-of-friends (FOF) algorithm integrated into Gizmo, based on

Gadget-3, with a linking length of 0.2 times the mean inter-particle separation. The YT-based package CAESAR² is then used in post-processing to cross-match galaxies and halos and generate a catalogue of pre-computed properties. Additionally, galaxies are identified using a 6-D FOF galaxy finder with a spatial linking length of 0.0056 times the mean inter-particle separation (twice the minimum softening kernel) and a velocity linking length set to the local velocity dispersion. This is applied to all stars and ISM gas with $n_{\text{H}} > 0.13 \text{ cm}^{-2}$. The H I and H_2 fractions for individual gas elements are taken directly from the simulation, without post-processing. To compute the H I and H_2 contents of galaxies, each gas particle in a halo is assigned to the galaxy with the highest M_{baryon}/R^2 ratio, where M_{baryon} is the total baryonic mass and R is the distance from the particle to the galaxy's centre of mass. This ensures that cold gas, particularly H I can be assigned to a galaxy even if it is not part of its ISM, as H I can be significant even for gas with $n_{\text{H}} > 0.13 \text{ cm}^{-2}$. It is important to note that black holes and H I gas are assigned to the galaxy to which they are most gravitationally bound, with the most massive black hole particles being designated as the central black hole.

2.1 SIMBA feedback variants

This study utilises five variants of the SIMBA suite of hydrodynamic simulations, all initialised with identical conditions. Each simulation box spans a co-moving volume of $50 \text{ h}^{-1} \text{ Mpc}$ per side and contains an equal number of dark matter and gas particles, specifically 512^3 for each type, ensuring uniform mass resolution of $9.6 \times 10^7 M_{\odot}$ for the dark matter and $1.82 \times 10^7 M_{\odot}$ the gas particles. This corresponds to an H I mass resolution of $\sim 10^8 M_{\odot}$. The cosmological framework for these simulations aligns with the Planck-16 ΛCDM model, characterised by parameters: $\Omega_m = 0.3$, $\Omega_{\Lambda} = 0.7$, $\Omega_b = 0.048$, $h = 0.68$, $\sigma_8 = 0.82$ and $n_s = 0.97$. The s50 simulation serves as the fiducial run, incorporating all features outlined in Section (2). The other four runs progressively deactivate the feedback modules, as summarised in Table 1. The s50noX run excludes only the X-ray mode, while the s50nojet run deactivates both jets and X-ray heating. In the s50noAGN run, all AGN feedback modes are turned off, leaving only stellar feedback processes active. Lastly, the s50nofb run, all feedback mechanisms- including both stellar and AGN feedback- are turned off. It is important to note that SIMBA still spawns black holes and includes metal cooling. Clarify that only stellar and AGN feedback is removed, not cooling, enrichment or H_2 formation. It is important to note that both the s50nofb and s50noAGN runs still include black hole seeds and the dual accretion mode. Due to the self-regulation of the torque-limited accretion mode (as described in Anglés-Alcázar et al. (2017); Davé et al. (2019)), black hole-galaxy scaling relations remain intact, even when combined with Bondi accretion and without feedback. For this study, only the $z = 0$ snapshot from each of the five runs is used.

3 METHODS

In this work, we adopt an approach that provides a more observationally consistent method for measuring the H I masses and sizes of galaxies, ensuring that our results are more directly comparable to empirical studies by minimising potential biases arising from

¹ X-ray feedback injects thermal energy into diffuse gas and a mix of kinetic and thermal energy into dense ISM gas

² <https://caesar.readthedocs.io/en/latest>

Table 1. Summary of feedback prescriptions used in the simulation runs. Each column represents a specific feedback mechanism—stellar feedback, AGN winds, AGN jets, and X-ray heating. A check mark (✓) indicates that the corresponding mechanism is included in a given run, while a dash (–) denotes its absence. Rows correspond to individual simulation runs, as described in the manuscript.

Name	Feedback Prescriptions			
	Stellar	AGN Winds	AGN Jet	X-ray Heating
s50	✓	✓	✓	✓
s50noX	✓	✓	✓	–
s50nojet	✓	✓	–	–
s50noAGN	✓	–	–	–
s50nofb	–	–	–	–

differences in measurement techniques. While directly using SIMBA particle lists offers a theoretically precise measure, it arguably lacks the observational realism necessary for a meaningful comparison.

For each galaxy in our samples, we use the MARTINI (Mock APERTIF-like Radio Telescope Interferometry of the Neutral ISM) package (Oman et al. 2019; Oman 2019, 2024) to generate a synthetic H I line data cube and derive an H I total intensity map. All cubes have a spatial pixel size of 8 arcseconds, and a Gaussian point-spread function with a half-power width of 24 arcseconds is applied for spatial smoothing. A fixed distance of 4 Mpc is assumed for all galaxies. The H I disc of each galaxy is inclined at 60 degrees to the y-axis in all cubes. Martini attempts to determine a preferred disc plane for each galaxy based on the angular momenta of the central one-third of its particles. Once an H I data cube is generated, its flux is spectrally integrated to produce a total intensity map. After converting the map’s pixel units from Jy/beam to $M_{\odot} \text{ pc}^{-2}$, we identify a thin mass surface density contour centered on $\sim 1 M_{\odot} \text{ pc}^{-2}$ and fit it with an ellipse. The major axis of the fitted ellipse defines the galaxy’s H I diameter, while the H I mass is obtained by summing the flux of all pixels with a surface density $\geq 1 M_{\odot} \text{ pc}^{-2}$. To identify galaxies with outer H I distributions too disturbed to yield reliable size estimates, we compute a quality-of-fit parameter for each fitted ellipse. For every point along the ellipse, we calculate its distance to the nearest map pixel³. The mean of these distances is then normalised by the semi-major axis of the fitted ellipse, providing a relative measure of fit quality. In Section 4, we describe how this quality parameter is used to refine our galaxy samples. Fig. 1 presents the H I total intensity maps and fitted ellipses for 20 galaxies that uniformly span the mass range $8 \leq \log_{10} \left(\frac{M_{\text{HI}}}{M_{\odot}} \right) \leq 10$ from the full-physics (s50) run, ordered by increasing H I mass.

4 SAMPLE

To create a suitable sample, we use the CAESAR-computed galaxy properties to select a subset best suited for measuring the quantities required to construct the H I MSR. Previous studies such as Glowacki et al. (2020, 2021); Elson et al. (2023) applied stellar and H I mass cuts of $M_{*} > 7.25 \times 10^8 M_{\odot}$ and $M_{\text{HI}} > 1.25 \times 10^8 M_{\odot}$, respectively. These cuts ensure that galaxies from the 25 Mpc³ SIMBA run are well above the mass resolution limit, making their measured properties accurate and reliable. In this work, we apply the same mass cuts

to galaxies in the 50 Mpc³ runs, even though their typical mass resolutions are expected to be significantly higher. This allows us to explore how far below the expected resolution limit our measured H I MSR extends. However, when parametrising the relation, we adopt more appropriate mass limits. Further details are provided in Section (5).

To minimise the impact of galaxy–galaxy interactions on our H I measurements, we exclude all galaxies with at least one neighbour within ~ 30 kpc. Additionally, to ensure our sample consists primarily of galaxies with extended, regular, rotating H I discs, we impose a dynamical morphology cut. Following Sales et al. (2012), we define:

$$\kappa_{\text{rot}} = \frac{K_{\text{rot}}}{K}, \quad (1)$$

where K_{rot} is the kinetic energy in ordered rotation and K is the total kinetic energy of the galaxy. We retain only galaxies with $\kappa_{\text{rot}} > 0.8$, as measured for their H I component.

As described in Section (3), each galaxy is fitted with an ellipse along a thin mass surface density contour centered on $\sim 1 M_{\odot} \text{ pc}^{-2}$. We retain only those galaxies for which the mean deviation between the ellipse and the contour is less than 5% of the semi-major axis length. This selection criterion effectively removes galaxies with significantly disturbed outer H I discs.

For each of the 50 Mpc³ runs used in this study, Fig. 2 shows the distribution of various galaxy properties. The blue histograms represent the full galaxy sample, while the orange histograms correspond to the subset used to generate the H I MSR.

In the s50 run, the stellar and H I mass distributions are relatively narrow and centered around $\sim 10^{9-10} M_{\odot}$, reflecting a self-regulated galaxy population. In contrast, runs lacking one or more key feedback prescriptions—such as AGN winds, jets, or X-ray feedback—exhibit broader distributions with extended tails toward both higher and lower masses. For example, the s50nofb variant shows a clear shift to lower H I masses, as the absence of feedback allows for excessive cooling. Gas fractions also vary significantly: runs with full feedback maintain moderate, balanced gas reservoirs, while feedback-deficient runs display extreme values due to either rapid gas consumption or inefficient gas retention. Additionally, galaxies in the no-feedback variants tend to be more compact and show a wider spread in star formation rates—from bursty to quenched—compared to the more uniform 2–5 kpc half-light radius and moderate star formation rates seen in the full-physics sample. All of these trends exemplify the expected impact of missing feedback: without proper regulation, galaxies can form across a wider range of masses and exhibit more diverse gas content, sizes, and star formation histories. The main aim of this study is to determine the resilience of the H I MSR to these differences.

5 RESULTS

Fig. (3) presents the fitted H I diameters as a function of H I mass for the five simulation variants. Galaxies in the SIMBA 50 Mpc/h boxes simulations are well resolved at $\log_{10}(M_{\text{HI}}/M_{\odot}) \geq 9$. The resolution limit for the 25 Mpc/h box is approximately $1.25 \times 10^8 M_{\odot}$, which is eight times finer than that of the 50 Mpc/h box, where the corresponding limit is therefore expected to be close to $1 \times 10^9 M_{\odot}$. To ensure a reliable fit to the H I MSR, we adopt a conservative

³ Within the thin mass surface density contour centred on $1 M_{\odot} \text{ pc}^{-2}$.

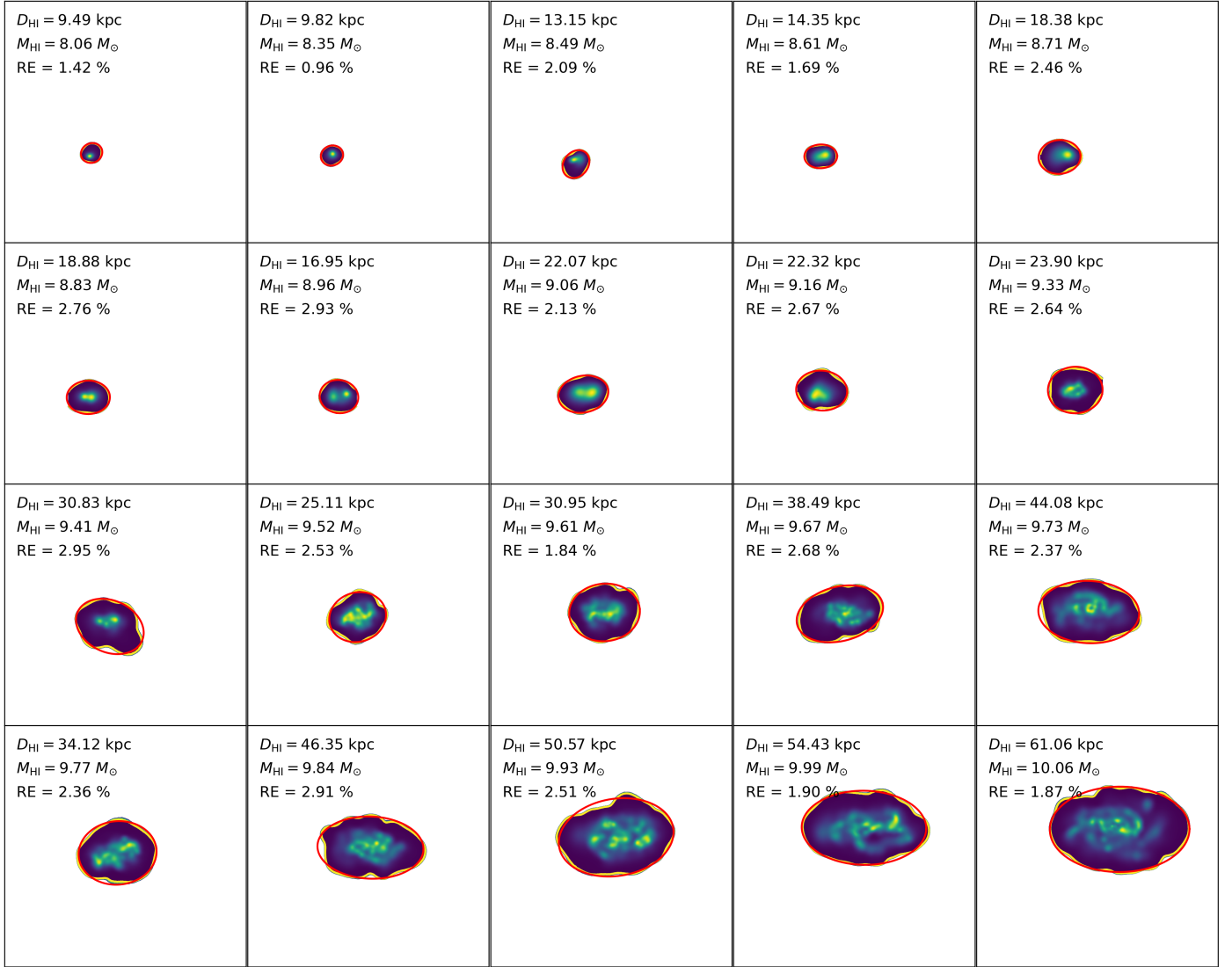


Figure 1. Twenty selected H I total intensity maps of galaxies from the full-physics (s50) run. The H I mass increases from left to right and top to bottom. The yellow contour in each panel marks the $1 M_{\odot} \text{ pc}^{-2}$ surface density level, while the fitted ellipse is shown in red. The text in each panel provides the physical size of the fitted ellipse, the galaxy’s total H I mass, and the relative error percentage, $\Delta D_{\text{HI}}/D_{\text{HI}}$, between the fitted ellipse and the $1 M_{\odot} \text{ pc}^{-2}$ density contour.

threshold of $\log_{10}(M_{\text{HI}}[M_{\odot}]) \geq 9.1$, providing a small, additional safety margin above the resolution limit. This criterion increases the chances that galaxies included in the H I SMR are well resolved (numerically), minimising biases from under-resolved systems and enabling a robust characterisation of the relation across the full sample.

Overlaid on each panel is the best-fitting power-law model for our fits.

$$\log_{10} \left(\frac{D_{\text{HI}}}{\text{kpc}} \right) = \alpha \cdot \log_{10} \left(\frac{M_{\text{HI}}}{M_{\odot}} \right) - \beta, \quad (2)$$

Obtained via Orthogonal Distance Regression (ODR; [Brown and Fuller 1990](#)), which minimizes perpendicular distance by accounting for errors in both variables. We quantify the model’s performance using the root-mean-square perpendicular distance (for galaxies above the $10^{9.1} M_{\odot}$ threshold. Table (2) summarized the best-fitting

parameters and the associated scatters.)

Also shown in each panel (blue solid line) is the empirical H I SMR from [Wang \(2016\)](#). When fitting Eqn (2) to all galaxies with $\log_{10} \left(\frac{M_{\text{HI}}}{M_{\odot}} \right) \geq 9.1$. All simulation runs agree well with the empirical relation despite the absence of certain feedback prescriptions. In the following section, we discuss why these relations persist.

6 DISCUSSION

The H I SMR has been shown to be well described by a single power-law spanning a wide range of H I masses (e.g. [Wang 2016](#)). This apparent universality is often interpreted as evidence for the self-similarity in the spatial distribution of gas within galaxies, where similar physical processes govern both the acquisition and distribution of H I irrespective of galaxy size or mass. Analytical

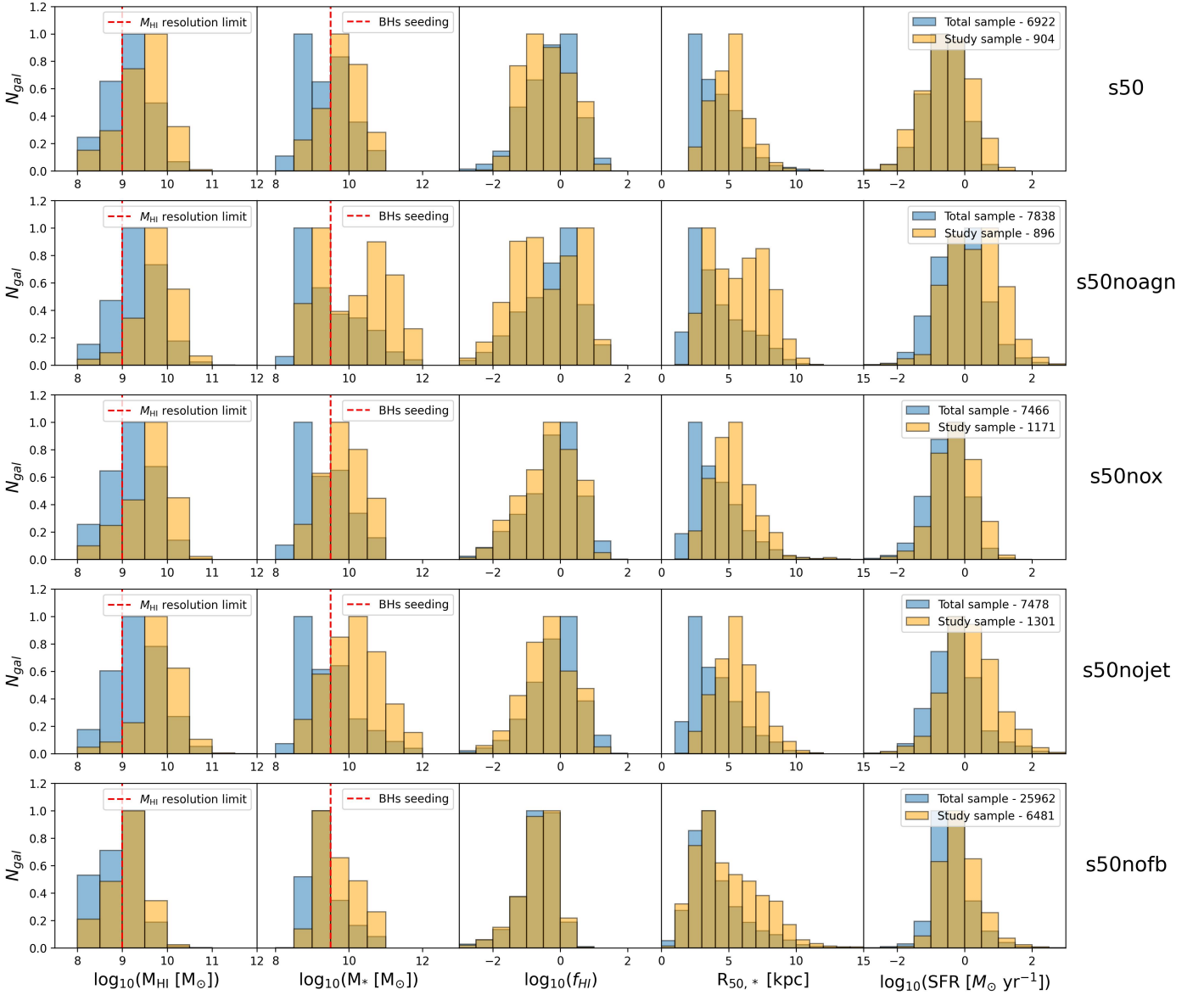


Figure 2. Distributions of key galaxy properties—logarithmic $H\text{I}$ mass, stellar mass, $H\text{I}$ fraction, and stellar half-mass radius—are shown for five simulation variants: s50, s50noAGN, s50noX, s50nojet, and s50nofb. In each panel, histograms compare the full galaxy sample (blue) with the selected study sample (orange). The variant name is indicated to the right of each row. The fourth panel also includes the number of galaxies in each sample. Vertical red dashed lines denote resolution limits: $M_{H\text{I}} > 10^{9.1} M_{\odot}$ for $H\text{I}$ mass and $M_* > 10^{9.5} M_{\odot}$, the threshold in SIMBA where black holes are seeded once a galaxy reaches this stellar mass limit, the latter corresponding to the stellar mass threshold in Simba above which black holes are seeded. Bin sizes are 0.5 dex for all properties except $R_{50,*}$ which uses 1 dex bins.

Table 2. $H\text{I}$ MSR fits to our sample of 50 Mpc^3 box for the different feedback variants.

	Wang et al 2016	s50	s50nox	s50nojet	s50noagn	s50nofb
Sample	562	904	1171	1301	896	6481
α	0.506 ± 0.003	0.504 ± 0.010	0.530 ± 0.008	0.522 ± 0.006	0.506 ± 0.009	0.531 ± 0.006
β	-3.293 ± 0.009	-3.279 ± 0.093	-3.541 ± 0.075	-3.458 ± 0.059	-3.294 ± 0.085	-3.507 ± 0.056
σ [dex]	0.06	0.096	0.103	0.083	0.097	0.122

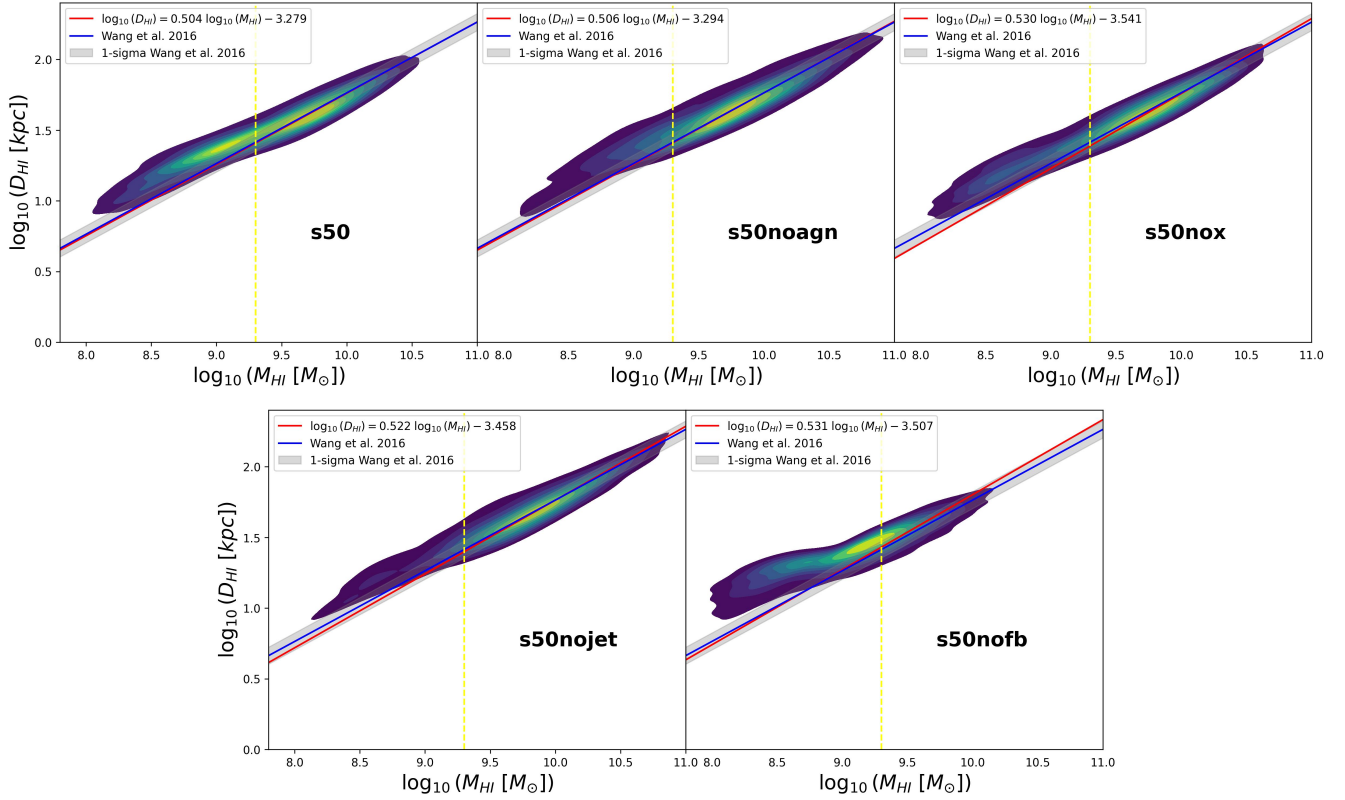


Figure 3. This plot represents 5 different H I mass-size relations (H I MSR) from the SIMBA-50 feedback variants. Each subplot shows the kernel density estimate (KDE) of the data with a colour map, along with the linear best-fit line (in red) derived from orthogonal distance regression (ODR) algorithm. The blue line represents the relation from Wang (2016), with the grey shaded region indicating the 1σ uncertainty of their fit. A vertical dashed line at $\log_{10}(M_{\text{HI}}[M_{\odot}]) = 9.1$ marks the threshold at which the best-fit line is fitted.

work by Stevens et al. (2019) demonstrates that when H I mass distributions exhibit self-similarity—particularly in their outer radial regions—a natural scaling arises between total H I content and spatial extent. Observational studies by Broeils & Rhee (1997); Verheijen (2001); Wang (2016) and Nalumsa, Elson, & Jarrett (2021) further support this interpretation, showing that the tightness of the relation is likely underpinned by the structural uniformity of H I discs.

Here, we investigate whether a similar self-similarity holds for the different samples of SIMBA galaxies, all of which have been shown to yield similar H I MSRs. For each galaxy in a given sample, the orientation parameters of its best-fitting ellipse⁴ are used to divide its H I total intensity map into concentric elliptical rings. The H I flux in each ring is azimuthally averaged to generate a radial mass profile. Each profile is then normalised in radius by the galaxy’s measured, R_{HI} . Galaxies are grouped into H I mass bins of width 0.25 dex over the range $\log(M_{\text{HI}}/M_{\odot}) = 8\text{--}10.75$, and within each bin, the radial profiles are averaged.

From left to right and top to bottom, the panels in Fig. 4, show the H I radial profiles normalised in radius from the various SIMBA 50 Mpc runs. In each panel, grey curves represent the profiles of individual galaxies in the give mass bin, while the red curve represents the mean profile. In this study we model each mean H I radial profile as a piecewise linear function comprising two seg-

ments—representing the inner and outer parts—naturally capturing the turnover radius, R_{turn} . This is modelled using the PWLF Python package, with the resulting fits shown as blue lines in Fig. 4 the corresponding turnover radius, R_{turn} , is indicated by the dashed green line.

The panels in Fig. 5 show the mean H I radial profiles for the different galaxy samples of the different runs, arranged in order of increasing H I mass. It is evident from Fig. 5 that across all mass bins, the mean radial profiles of the various runs differ somewhat at small radii ($R/R_{\text{HI}} \lesssim 0.5$), but tend to converge at larger radii, $R/R_{\text{HI}} > 0.5$. Specifically, the outer profiles are well described by exponential functions with similar rates of decline whereas the inner profiles tend to be more constant with possible depressions at the center. For the outer segments, we extract the fitted gradients and plot them as a function of H I mass in Fig. 6. While the slope of the outer profiles gradually decreases with increasing H I mass, it remains highly consistent across all physics runs at fixed H I mass. The outer H I distributions of SIMBA galaxies are therefore quantifiably self-similar, which we interpret as the underlying reason why the H I MSR remains robust across different feedback implementations.

In contrast to results from the EAGLE simulation (Crain et al. 2015; Schaye et al. 2015)—where strong feedback mechanisms led to central H I depressions and notable deviations in the H I MSR (Bahé et al. 2016)—our findings reveal no such anomalies, even when individual feedback modes are disabled. Both the H I MSRs and the H I radial profiles remain closely aligned across all scenarios

⁴ Used to measure its diameter for the H I MSR.

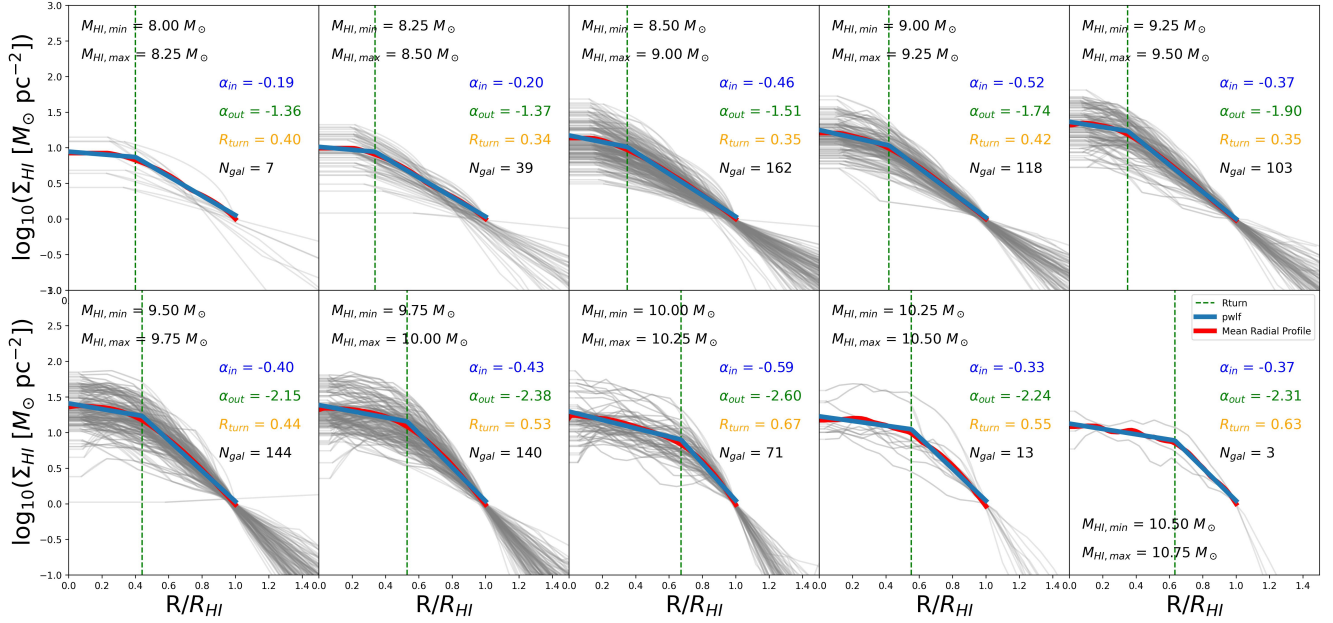


Figure 4. The scaled H I radial profiles from the SIMBA-50 $z = 0$ are shown. These profiles are scaled to R_{HI} , and by definition, they overlap at a surface density of $\Sigma_{\text{HI}} = 1 M_{\odot} \text{pc}^{-2}$. Each panel corresponds to a different mass bins, with a width of 0.25 in log-scale, covering the range $\log_{10}(M_{\text{HI}}) = [8, 10.75]$. The number of galaxies per mass bin is denoted as N_{gal} . The grey lines represent the individual galaxy profiles, the red line shows the mean H I radial profile. The green dashed line indicates R_{turn} , the turning point that separates the inner and outer regions of the H I profiles. The blue line represents the fit to the mean H I radial profile, obtained using the piecewise linear fitting (PWLF) method in Python. α_{in} and α_{out} represents the inner and outer slopes.

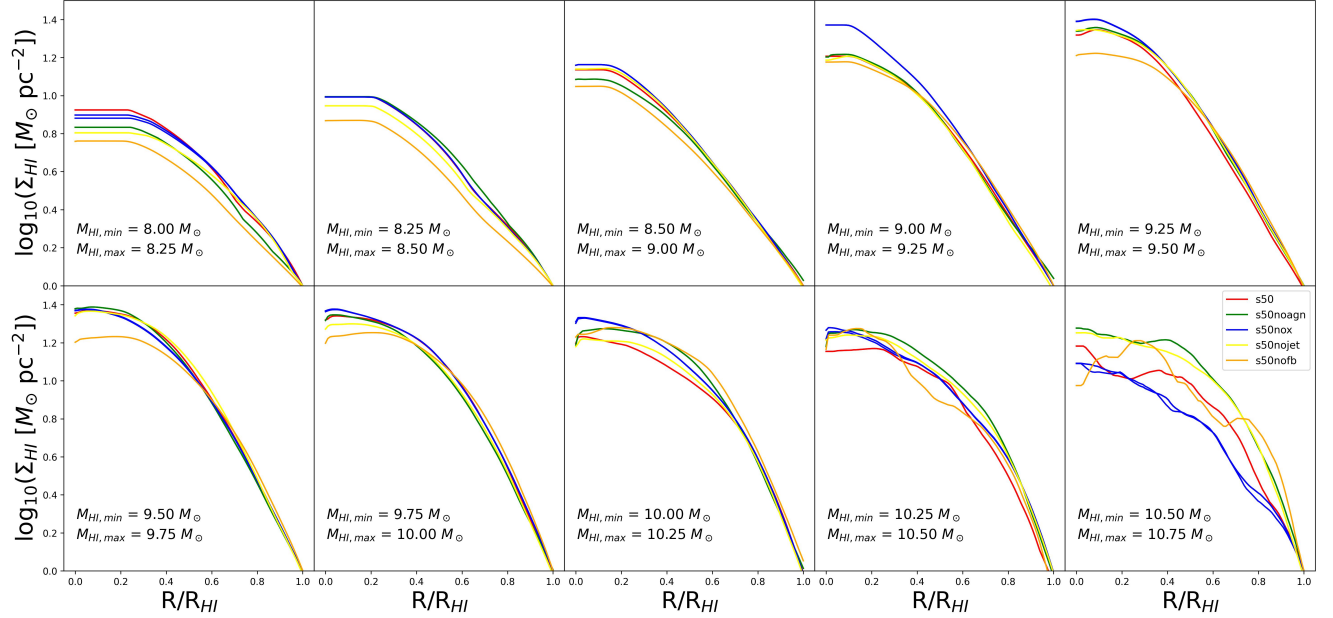


Figure 5. The scaled mean H I radial profiles from the SIMBA-50 simulation at $z=0$ for different feedback variants. When normalised by each galaxy's characteristic H I disc size, the profiles reveal a universal exponential shape across all H I mass bins and feedback scenarios, highlighting the self-similarity of the outer H I distributions regardless of feedback strength.

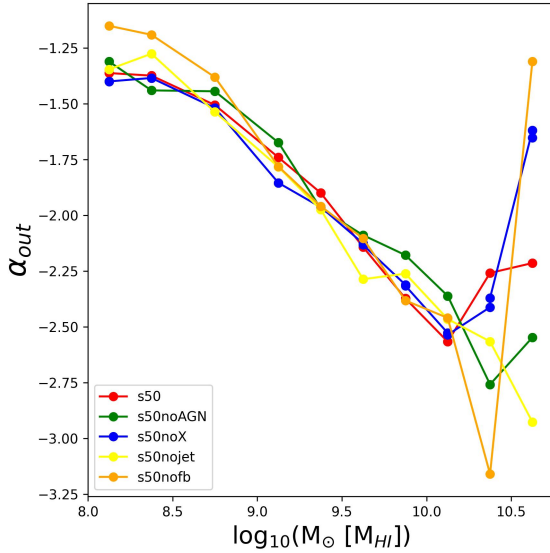


Figure 6. The outer slope as a functions of the mass bin midpoint for different simulation variants. This figure illustrates that the outer slope steepens with increasing mass, with feedback mechanisms influencing the rate of decline, but the behaviour is generally in agreement for $\log_{10}(M_{\text{HI}}[M_{\odot}]) < 10.1$. The s50nofb case consistently shows the most extreme trends, highlighting the crucial role of feedback in shaping galaxy structure.

, with only minor variations, mostly in terms of scatter. This consistency strengthens the case that galaxies adhere to the observed H I MSR irrespective of feedback strength. In semi-analytic models with resolved disc structure – Fu et al. (2013), the universal shape of outer gas discs has been attributed to assumptions of exponentially declining gas infall and the “inside-out” formation of discs (Wang et al. 2014). Feedback is expected to modulate this growth by regulating the availability of cold gas, thereby influencing the pace and nature of inside-out evolution (Baker et al. 2025). As many galaxy formation models adopt an exponential form for the H I surface density profile, they naturally reproduce similar mass–size scalings (Stevens et al. 2019).

The persistence of the H I MSR across the various SIMBA runs may stem from the standard methodology used to define H I disc extents. Typically, a surface density threshold of $1 M_{\odot} \text{ pc}^{-2}$ is adopted, corresponding to galactocentric radii of several kiloparsecs. At these scales, the gas lies beyond the immediate influence of AGN-driven feedback from the galactic centre, thereby preserving the integrity of the H I MSR. Moreover, this contour generally encloses regions deep within the galaxy’s gravitational potential, where H I is relatively stable against environmental processes such as ram-pressure stripping. However, at lower surface density thresholds (e.g. 0.1 or $0.01 M_{\odot} \text{ pc}^{-2}$), where the H I is more weakly bound, external perturbations are expected to play a more prominent role. Investigating potential deviations in the H I MSR within these low-density regimes is deferred to future work.

7 CONCLUSION

We investigate the potential impact of different feedback mechanisms on the H I size–mass relation (H I MSR) using the SIMBA suite of cosmological hydrodynamical simulations at $z = 0$. These simulations incorporate both stellar and AGN-driven feedback

processes in the 50 Mpc^3 box. Our analysis considers four feedback variants: the s50noX run, which excludes only the AGN X-ray feedback mode; s50nojet, which disables both AGN jets and X-ray heating; s50noAGN, which removes all AGN feedback modes, retaining only stellar feedback; and s50nofb, where all feedback processes are turned off.

We find that the H I MSR remains remarkably consistent across all feedback implementations, indicating that the relation for SIMBA galaxies is not strongly regulated by the presence or absence of AGN or stellar feedback. To explore the origin of this invariance, we analyse the azimuthally averaged radial H I surface density profiles for galaxies in each simulation. While mild variations are present at small radii, the profiles converge at larger radii to a common, self-similar exponential form. The outer profile slopes show minimal variation at fixed H I mass across all feedback scenarios, reinforcing the conclusion that the structural uniformity of outer H I discs underlies the observed stability of the H I MSR.

DATA AVAILABILITY

Measurement quantities will be made available upon reasonable request.

REFERENCES

- Anglés-Alcázar D., Faucher-Giguère C.-A., Quataert E., Hopkins P. F., Feldmann R., Torrey P., Wetzel A., Kereš D., 2017, Black holes on FIRE: stellar feedback limits early feeding of galactic nuclei, *Monthly Notices of the Royal Astronomical Society: Letters*, 472(1), L109–L114.
- Bahé Y. M., Crain R. A., Kauffmann G., Bower R. G., Schaye J., Furlong M., Lagos C., Schaller M., Trayford J. W., Dalla Vecchia C., et al., 2016, The Distribution of Atomic Hydrogen in EAGLE Galaxies: Morphologies, Profiles, and H I Holes, *Monthly Notices of the Royal Astronomical Society*, 456, 1115–1136.
- Baker W. M., Tacchella S., Johnson B. D., Nelson E., Suess K. A., D’Eugenio F., Curti M., de Graaff A., Ji Z., Maiolino R., et al., 2025, *Nature Astronomy*, 9, 141–154, A core in a star-forming disc as evidence of inside-out growth in the early Universe
- Broeils A. H., van Woerden H., 1994, A Search for Spiral Galaxies with Extended H I Disks, *Astronomy and Astrophysics Supplement Series*, 107, 129–176.
- Broeils A. H., Rhee M.-H., 1997, Short 21-cm WSRT Observations of Spiral and Irregular Galaxies. H I Properties, *Astronomy and Astrophysics*, 324, 877–887.
- Brown P. J., Fuller W. A., 1990, *Statistical analysis of measurement error models and applications: Proceedings of the AMS-IMS-SIAM joint summer research conference held June 10-16, 1989, with support from the National Science Foundation and the US Army Research Office*, vol. 112, American Mathematical Soc.
- Cayatte V., Kotanyi C., Balkowski Ch., van Gorkom J. H., 1994, A Very Large Array Survey of Neutral Hydrogen in Virgo Cluster Spirals. III: Surface Density Profiles of the Gas, *Astronomical Journal*, 107, 1003–1017.
- Choi E., Ostriker J. P., Naab T., Johansson P. H., 2012, *ApJ*, 754, 125
- Christiansen J. F., Davé R., Sorini D., Anglés-Alcázar D., 2020, Jet feedback and the photon underproduction crisis in SIMBA, *Monthly Notices of the Royal Astronomical Society*, 499(2), 2617–2635.
- Crain R. A., Schaye J., Bower R. G., Furlong M., Schaller M., Theuns T., Dalla Vecchia C., Frenk C. S., McCarthy I. G., Helly J. C., et al., 2015, The EAGLE Simulations of Galaxy Formation: Calibration of Subgrid Physics and Model Variations, *Monthly Notices of the Royal Astronomical Society*, 450, 1937–1961.

- Davé R., Thompson R., Hopkins P. F., 2016, MUFASA: galaxy formation simulations with meshless hydrodynamics, *MNRAS*, 462, 3265–3284.
- Davé R., Anglés-Alcázar D., Narayanan D., Li Q., Rafieferantsoa M. H., Appleby S., 2019, SIMBA: Cosmological simulations with black hole growth and feedback, *Monthly Notices of the Royal Astronomical Society*, 486(2), 2827–2849.
- Davé R., Crain R. A., Stevens A. R. H., Narayanan D., Saintonge A., Catinella B., Cortese L., 2020, Galaxy cold gas contents in modern cosmological hydrodynamic simulations, *Monthly Notices of the Royal Astronomical Society*, 497(1), 146–166.
- Elson E., Glowacki M., Davé R., 2023, Measurements of the angular momentum–mass relations in the Simba simulation, *New Astronomy*, 99, 101964.
- Fu J., Kauffmann G., Huang M.-L., Yates R. M., Moran S., Heckman T. M., Davé R., Guo Q., Henriques B. M. B., 2013, Star Formation and Metallicity Gradients in Semi-analytic Models of Disc Galaxy Formation, *Monthly Notices of the Royal Astronomical Society*, 434, 1531–1548.
- Glowacki M., Elson E., Davé R., 2020, The baryonic Tully–Fisher relation in the SIMBA simulation, *Monthly Notices of the Royal Astronomical Society*, 498(3), 3687–3702.
- Glowacki M., Elson E., Davé R., 2021, The redshift evolution of the baryonic Tully–Fisher relation in SIMBA, *Monthly Notices of the Royal Astronomical Society*, 507(3), 3267–3284.
- Heckman T. M., Best P. N., 2014, The coevolution of galaxies and super-massive black holes: insights from surveys of the contemporary universe, *Annual Review of Astronomy and Astrophysics*, 52, 589.
- Hopkins P. F., 2015, A new class of accurate, mesh-free hydrodynamic simulation methods, *Monthly Notices of the Royal Astronomical Society*, 450(1), 53–110.
- Khrykin I. S., Sorini D., Lee K.-G., Davé R., 2024, The cosmic baryon partition between the IGM and CGM in the SIMBA simulations, *Monthly Notices of the Royal Astronomical Society*, 529(1), 537–549.
- Nalumsa E., Elson E. C., Jarrett T. H., 2021, *MNRAS*, 502, 5711–5725, H I global scaling relations in the WISE-WHISP survey
- Obreschkow D., Croton D., De Lucia G., Khochfar S., Rawlings S., 2009, Simulation of the cosmic evolution of atomic and molecular hydrogen in galaxies, *Astrophysical Journal*, 698, 1467.
- Oman K. A., Marasco A., Navarro J. F., Frenk C. S., Schaye J., Benítez-Llambay A., 2019, *MNRAS*, 482, 821
- Oman K. A., 2019, MARTINI: Mock spatially resolved spectral line observations of simulated galaxies, Astrophysics Source Code Library, record ascl:1911.005 (ascl:1911.005)
- Oman K., 2024, *The Journal of Open Source Software*, 9, 6860
- Rahmati A., Pawlik A. H., Raičević, M., Schaye J., 2013, On the evolution of the H I column density distribution in cosmological simulations, *Monthly Notices of the Royal Astronomical Society*, 430(3), 2427–2445.
- Sales L. V., Navarro J. F., Theuns T., Schaye J., White S. D. M., Frenk C. S., Crain R. A., Dalla Vecchia C., 2012, The origin of discs and spheroids in simulated galaxies, *Monthly Notices of the Royal Astronomical Society*, 423(2), 1544–1555.
- Schaye J., Crain R. A., Bower R. G., Furlong M., Schaller M., Theuns T., Dalla Vecchia C., Frenk C. S., McCarthy I. G., Helly J. C., et al., 2015, The EAGLE Project: Simulating the Evolution and Assembly of Galaxies and Their Environments, *Monthly Notices of the Royal Astronomical Society*, 446, 521–554.
- Smith B. D., Bryan G. L., Glover S. C. O., Goldbaum N. J., Turk M. J., Regan J., Wise J. H., Schive H.-Y., Abel T., Emerick A., 2017, GRACKLE: a chemistry and cooling library for astrophysics, *Monthly Notices of the Royal Astronomical Society*, 466(2), 2217–2234.
- Stevens A. R. H., Diemer B., Lagos C. d. P., Nelson D., Obreschkow D., Wang J., Marinacci F., 2019, Origin of the Galaxy H I Size–Mass Relation, *Monthly Notices of the Royal Astronomical Society*, 490, 96–113.
- Swaters R. A., van Albada T. S., van der Hulst J. M., Sancisi R., 2002, The Westerbork HI survey of spiral and irregular galaxies–I. HI imaging of late-type dwarf galaxies, *Astron. Astrophys.*, 390, 829–861
- Verheijen M. A. W., 2001, The Ursa Major Cluster of Galaxies. V. H I Rotation Curve Shapes and the Tully–Fisher Relations, *The Astrophysical Journal*, 563(2), 694.
- Ward S. R., Harrison C. M., Costa T., Mainieri V., 2022, Cosmological simulations predict that AGN preferentially live in gas-rich, star-forming galaxies despite effective feedback, *Monthly Notices of the Royal Astronomical Society*, 514(2), 2936–2957.
- Wang J., Fu J., Aumer M., Kauffmann G., Józsa G. I. G., Serra P., Huang M.-L., Brinchmann J., van der Hulst T., Bigiel F., 2014, An Observational and Theoretical View of the Radial Distribution of H I Gas in Galaxies, *Monthly Notices of the Royal Astronomical Society*, 441, 2159–2172.
- Wang J., 2016, The H I size-mass relation of galaxies, *Proceedings of the International Astronomical Union*, 11(S321), 284–284.

This paper has been typeset from a \LaTeX file prepared by the author.